LAWRENCE
LIVERMORE
NATIONAL
LABORATORY

UCRL-PROC-225822

Simulation of Turbulent Combustion Fields of Shock-Dispersed Aluminum Using the AMR Code

A. L. Kuhl, J. B. Bell, V. E. Beckner, B. Khasainov

November 3, 2006

41st Combustion Subcommittee/29th Airbreathing Propulsion Subcommittee and 23rd Propulsion Systems Hazards Subcommitte
San Diego, CA, United States
December 4, 2006 through December 8, 2006

DISCLAIMER

This work was performed under the auspices of the U.S. Department of Energy by the University of California, Lawrence Livermore National Laboratory under Contract No. W-7405-Eng-48.

SIMULATION OF TURBULENT COMBUSTION FIELDS

OF SHOCK-DISPERSED ALUMINUM USING THE AMR CODE*

A. L. Kuhl
University of California Lawrence Livermore National Laboratory
Livermore, California

J. B. Bell and V. E. Beckner
University of California Lawrence Berkeley National Laboratory
Berkeley, California

B. Khasainov
Laboratoire de Combustion et Detonique
Futuroscope (Poitiers), France

ABSTRACT

We present a Model for simulating experiments of combustion in Shock-Dispersed-Fuel (SDF) explosions. The SDF charge consisted of a 0.5-g spherical PETN booster, surrounded by 1-g of fuel powder (flake Aluminum). Detonation of the booster charge creates a high-temperature, high-pressure source (PETN detonation products gases) that both disperses the fuel and heats it. Combustion ensues when the fuel mixes with air. The gas phase is governed by the gas-dynamic conservation laws, while the particle phase obeys the continuum mechanics laws for heterogeneous media. The two phases exchange mass, momentum and energy according to inter-phase interaction terms. The kinetics model used an empirical particle burn relation. The thermodynamic model considers the air, fuel and booster products to be of frozen composition, while the Al combustion products are assumed to be in equilibrium. The thermodynamic states were calculated by the Cheetah code; resulting state points were fit with analytic functions suitable for numerical simulations. Numerical simulations of combustion of an Aluminum SDF charge in a 6.4-liter chamber were performed. Computed pressure histories agree with measurements.

INTRODUCTION

We consider the explosion of a 0.5-g spherical PETN charge that disperses 1-g of flake Aluminum (Al) powder in a 6.6-l calorimeter as reported by Neuwald et al[1]. The Al powder is heated by the explosion products, and when the Al mixes with air, it releases 7,400 cal/g by a non-premixed turbulent combustion process[2]. Here we model the evolution of combustion in physical space by numerical simulations.

MODEL

GAS PHASE

We model evolution of the combustion field in the limit of large Reynolds and Peclet numbers, where molecular diffusion and heat conduction effects in the gas phase are negligible. The flow field is then governed by the gas-dynamic conservation laws:

Mass:
$$\partial_t \rho + \nabla \cdot (\rho \mathbf{u}) = \dot{\sigma}_s \qquad (1)$$

Approved for public release; distribution is unlimited.
* This effort was performed under IACRO # 06-40731 with the Defense Threat Reduction Agency.

Momentum: $$\partial_t \rho \mathbf{u} + \nabla \cdot (\rho \mathbf{u}\mathbf{u} + p) = \dot{\sigma}_s \mathbf{v} - \dot{f}_s \quad (2)$$

Energy: $$\partial_t \rho E + \nabla \cdot (\rho \mathbf{u} E + p\mathbf{u}) = -\dot{q}_s + \dot{\sigma}_s E_s - \dot{f}_s \cdot \mathbf{v} \quad (3)$$

where $\rho, p, \mathbf{u}$ represent the gas density, pressure and specific internal energy, **u** is the gas velocity vector, and $E \equiv u + \mathbf{u} \cdot \mathbf{u}/2$ denotes the total energy of the gas phase. Source terms on the right hand side take into account: mass addition to gas phase due to particle burning ($\dot{\sigma}_s$), particle drag ($\dot{f}_s$), and heat losses ($\dot{q}_s$).

PARTICLE PHASE

We treat the particle phase as continuum. We consider the dilute limit, devoid of particle-particle interactions, so that the pressure and sound speed of the particle phase are zero. We model the evolution of particle phase mass, momentum and energy fields by the conservation laws of continuum mechanics for heterogeneous media as described by Nigmatulin[3]:

Mass: $$\partial_t \sigma + \nabla \cdot \sigma \mathbf{v} = -\dot{\sigma}_s \quad (4)$$

Momentum: $$\partial_t \sigma \mathbf{v} + \nabla \cdot \sigma \mathbf{v}\mathbf{v} = -\dot{\sigma}_s \mathbf{v} + \dot{f}_s \quad (5)$$

Energy: $$\partial_t \sigma E_s + \nabla \cdot \sigma E_s \mathbf{v} = \dot{q}_s - \dot{\sigma}_s E_s + \dot{f}_s \cdot \mathbf{v} \quad (6)$$

Number particles: $$\partial_t n_s + \nabla \cdot n_s \mathbf{v} = 0 \quad (7)$$

where σ and **v** represent the particle-phase density and velocity while $E_s \equiv C_s T_s + \mathbf{v} \cdot \mathbf{v}/2$ denotes the total energy of the particle phase.

INTERACTION

The inter-phase interaction terms for mass, momentum, heat and particle burning law take the following form[4]:

Mass Exchange: $$\dot{\sigma}_s = \begin{cases} 0 & T_s < T_{ign} \\ -3\sigma(1 + 0.276\sqrt{\mathrm{Re}_s})/t_s & T_s \geq T_{ign} \end{cases} : \quad (8)$$

Momentum Exchange: $$\dot{f}_s = \frac{3}{4}\frac{\rho}{\rho_s}\frac{\sigma}{d_s} C_D (\mathbf{u} - \mathbf{v})|\mathbf{u} - \mathbf{v}| \quad (9)$$

where $C_D = 24/\mathrm{Re}_s + 4.4/\sqrt{\mathrm{Re}_s} + 0.42$ and $\mathrm{Re}_s = \rho d_s |\mathbf{u} - \mathbf{v}|/\mu$ (10)

Heat Exchange: $$\dot{q}_s = \frac{6\sigma}{\rho_s d_s}\left[\frac{Nu\lambda(T - T_s)}{d_s} + \varepsilon\sigma_{Boltz}(T^4 - T_s^4)\right] \quad (11)$$

where $Nu = 2 + 0.6\,\mathrm{Pr}\sqrt{\mathrm{Re}_s}$ (12)

Burning Law[5]: $$t_s = K d_{s0}^n / \phi^{0.9} \quad (13)$$

COMBUSTION

We consider three components: air (*A*), fuel (*F*) consisting of Al vapor, and equilibrium combustion products (*P*). They are governed by the following conservation laws:

Air-A: $$\partial_t \rho Y_{Air} + \nabla \cdot \rho Y_{Air} \mathbf{u} = -\alpha_s \dot{\sigma}_s \quad (14)$$

Fuel-F (metal vapor): $$\partial_t \sigma_F + \nabla \cdot \sigma_F \mathbf{u} = -\dot{\sigma}_s \quad (15)$$

Products-P: $$\partial_t \rho Y_P + \nabla \cdot \rho Y_P \mathbf{u} = (1 + \alpha_s)\dot{\sigma}_s \quad (16)$$

These are augmented by the conserved scalar equation:

Conserved Scalar: $$\partial_t(\sigma_F + \rho Y_{Air} + \rho Y_P) + \nabla\cdot(\sigma_F + \rho Y_{Air} + \rho Y_P)\,\mathbf{u} = 0 \qquad (17)$$

Fuel and air are consumed in stoichiometric proportions: $\alpha_s = air\,/\,fuel = 4.03$.

THERMODYNAMICS AND EQUATIONS OF STATE

The thermodynamic states encountered during the combustion of the aluminum powder with air are depicted by the Le Chatelier diagram[6,7] of Fig. 1. The Reactants-R are defined as a stoichometric mixture of air and Aluminum in *frozen* composition (air/fuel ratio: $\alpha_s = 4.03$). The Products-P are assumed to be in *thermodynamic equilibrium*. These states were calculated with the Cheetah code, assuming $p = 1\,atm$. Computations were also performed assuming combustion at $p = 10\,atm$; the resulting curve was negligibly different from the 1-atm curve for temperatures below 3,500K, so the 1-atm curve was adopted as the standard for this problem. Pressure independence is a perfect gas property, which seems to apply for the present combustion conditions. The heat of combustion is the difference between the energy of the products minus energy of reactants: $\Delta H_c \equiv u_{0,P} - u_{0,R} = -1{,}473 cal/g_P$ ($7{,}409\,cal/g_{Al}$) and is indicated on Fig. 1. Adiabatic combustion corresponds to a material transformation from Reactants to Products at constant energy. For Reactants starting at 300 K, this gives a combustion temperature of 3,680 K, as indicated in the figure. These states have been fit with quadratic functions:

$$u_k(T) = a_k T^2 + b_k T + c_k \quad (k = A, DP, R, P) \qquad (18)$$

These functions (curves) do an excellent job at fitting the computed thermodynamic states (data points) as demonstrated in Fig. 1 (see Appendix for values of a_k, b_k, c_k). Given the internal energy and composition Y_k in a cell, (18) can be solved to find the temperature. For a pure cell ($Y_k = 1$) one finds:

$$T_k = [-b_k + \sqrt{b_k^2 - 4a_k(c_k - u_k)}\,]/2a_k \qquad (19)$$

For computational cells containing a mixture of components, the *Intensive-variable Addition Law* is used to calculate the mixture energy:

$$u_m = \sum_k Y_k u_k = a_m T_m^2 + b_m T_m + c_m \qquad (20)$$

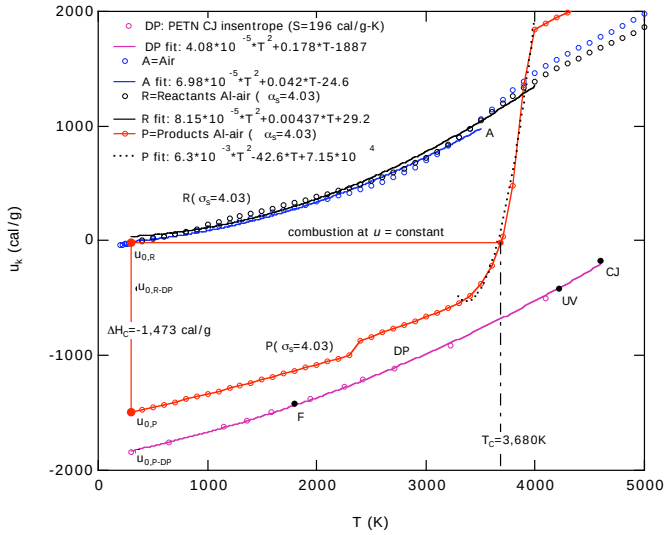

Figure 1. Le Chatelier diagram for stoichiometric combustion of aluminum in air ($\alpha_s = 4.03$). Adiabatic combustion corresponds to a material transformation from the Reactants-R to the Products-P at constant energy, represented as a horizontal line shown for reactants at 300K.

The mixture temperature is calculated from the inversion of (20):

$$T_m = [-b_m + \sqrt{b_m^2 - 4a_m(c_m - u_m)}]/2a_m \tag{21}$$

while the mixture properties are determined from:

$$a_m = \sum_k Y_k a_k\,, \quad b_m = \sum_k Y_k b_k\,, \quad c_m = \sum_k Y_k c_k\,, \quad R_m = \sum_k Y_k R_k \tag{22}$$

For pure cells ($Y_k = 1$) the pressure is calculated from the following:

$$p_k = \begin{cases} \rho_k R_k T_k & k = A, R, P \\ p_{JWL}(\rho, \mathrm{T}) & k = DP \end{cases} \tag{23}$$

In the above, the detonation products (DP) are described by the Jones-Wilkins-Lee (JWL) function:

$$p_{JWL}(\rho, T) = A\left[1 - \frac{\omega}{R_1 \mathrm{v}}\right]\exp(-R_1 \mathrm{v}) + B\left[1 - \frac{\omega}{R_1 \mathrm{v}}\right]\exp(-R_2 \mathrm{v}) + \rho R_{DP} T \tag{24}$$

where v represents the specific volume ratio: $\mathrm{v} = v / v_0 = \rho_0 / \rho$. For PETN at $\rho_0 = 1 g/cc$, the JWL constants are $A = 5.8$ M-bar; $B = 0.093$ M-bars; $C = 0.01223$ M-bars; $R_1 = 7.0$; $R_2 = 1.7$, $R_{DP} = 28.76$ g/g-mole and $\omega = \gamma - 1 = 0.246$. In mixed cells, the mixture pressure is calculated from the mixture temperature by the *Law of Additive Pressures*[8]:

$$p_m = \sum_k p_k(V_m, T_m) \tag{25}$$

where $p_k(V_m, T_m)$ denotes the pressure that would be exerted by component *k* if it existed alone at the temperature and volume of the mixture.

RESULTS AND DISCUSSION

Numerical simulations of the explosion of an Al-SDF charge (0.5-g PETN +1.0-g flake Al) in a 6.6-liter calorimeter were performed. We start by considering the initial blast wave expansion field. For times less than the first shock arrival at the calorimeter wall ($t \sim 80\,\mu s$), this flow field may be approximated as a one-dimensional (1D) spherical problem. The two-phase flow field profiles are presented in Figs. 2-5. Solid curves denote the gas phase while dashed curves represent the particle phase. Expansion of the charge drives a blast wave into the surrounding atmosphere (Fig. 2). Just after breakout, ($t = 5\,\mu s$) a 40 bar air shock is formed; this decays to a peak pressure of 10 bars as the shock approaches the wall ($R = 12\,cm$). Pressures near center ($R = 0$) approach zero due to the over-expansion of the detonation products gases. This creates a backward-facing shock evident at $R \sim 5cm$ which implodes at later times. These pressure waveforms are typical of HE-driven blasts, as was first predicted by Brode[9] in 1958.

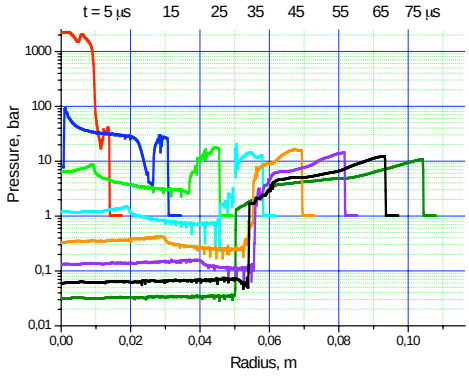

Figure 2. Pressure wave structure during the blast wave expansion phase.

The two-phase velocity profiles are presented in Fig. 3. The initial velocity profile of the gas phase peaks at 2,300 m/s. In $5\mu s$, this accelerates the particle phase to a peak velocity of 1,000 m/s. By $25\mu s$, the velocity fields of the two phases have equilibrated (green curves), with a peak of about 1,500 m/s. At later times the gas velocity field decays faster then the particle phase, so that at $t = 75\mu s$ the velocity of the particle phase is greater than that of the gas (1,000 m/s versus 800 m/s, respectively), indicating that the particle phase is accelerating the gas through drag interactions. In effect, the particle cloud acts as a leaky piston.

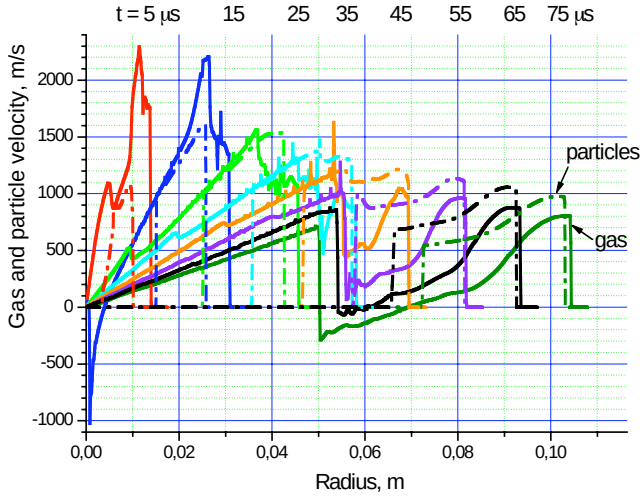

Figure 3. Two-phase velocity profiles during the blast wave expansion phase (solid curves denote gas phase and dashed curves denote particle phase).

The two-phase density profiles are presented in Fig. 4. The particle cloud starts with a peak density of 1,000 kg/m^3; at later times this decays to 1 kg/m^3, which is an order of magnitude smaller than the gas densities.

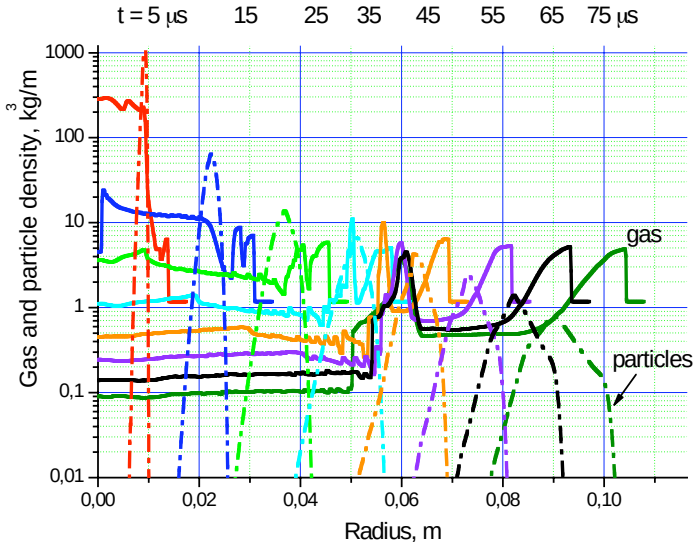

Figure 4. Two-phase density profiles during the blast wave expansion phase (solid curves denote gas phase and dashed curves denote particle phase).

The two-phase temperature profiles are depicted in Fig. 5. The initial gas temperature in the blast wave is about 2,500 K. By $5\,\mu s$, the air has heated the particle cloud to a temperature of 1,000 K (melting of Al at 933 K is seen at $t < 45\,\mu s$). After an induction time of about $35\,\mu s$, the Aluminum particles ignite. This Al-air combustion raises the temperature of the particle cloud to 2,500 K, thereby heating the surrounding air. So, at early times the air heats the particles, while at later times the particles heat the air (due to combustion effects).

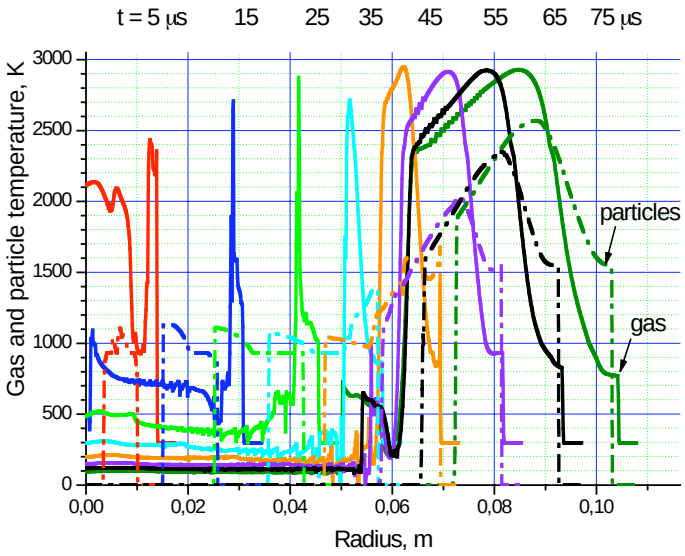

Figure 5. Two-phase temperature profiles during the blast wave expansion phase (solid curves denote gas phase and dashed curves denote particle phase).

Reynolds number profiles (based on the slip velocity and a mean particle diameter) are presented in Fig. 6. Characteristically the Reynolds numbers are very small ($0.01 < \mathrm{Re} < 0.1$)—indicating that gas flow among the particles is in the Stokes flow regime, where $C_D \sim 24/\mathrm{Re}$. At such small Reynolds numbers, the drag force is very large ($240 < C_D < 2{,}400$). This large drag causes the phases to rapidly equilibrate—so that the ensemble mixture behaves, in effect, as a dense fluid.

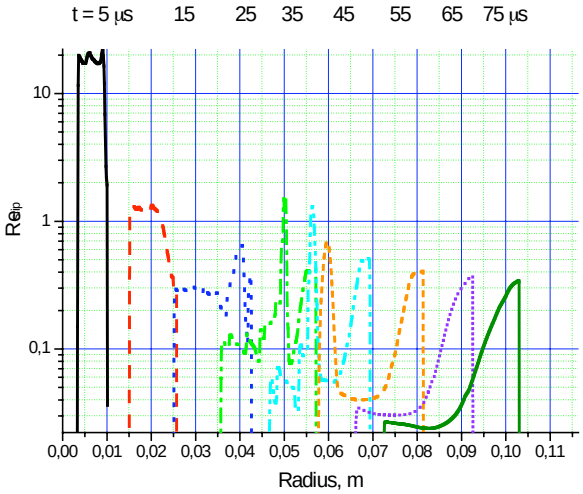

Figure 6. Two-phase Reynolds number profiles during the blast wave expansion phase.

Next a simulation was performed with the three-dimensional (3D) Cartesian-grid version of the AMR code[10,11]. In particular, the combustion of the Al-SDF charge in a 6.6-liter cylinder (L=21cm and H=20cm) was modeled in the equilibrium limit—thereby taking advantage of the observations noted in the preceding paragraph. A volume rendering of the combustion products surface at the beginning of the combustion process is presented in Fig. 7. It shows the initial development of instabilities on the products surface. Cross-sectional views of the Products concentration field and the temperature field are shown in Figs. 8, 9. They illustrate that the 3D AMR code can capture the turbulent mixing structures on the computational grid. These simulations implicitly incorporate the *MILES-type* (Monotone Integrated Large Eddy Simulation) representation of mixing, as promoted by Boris[12] — so no turbulence modeling is required. By using AMR, we capture the energy-bearing scales of the turbulence on the computational grid.

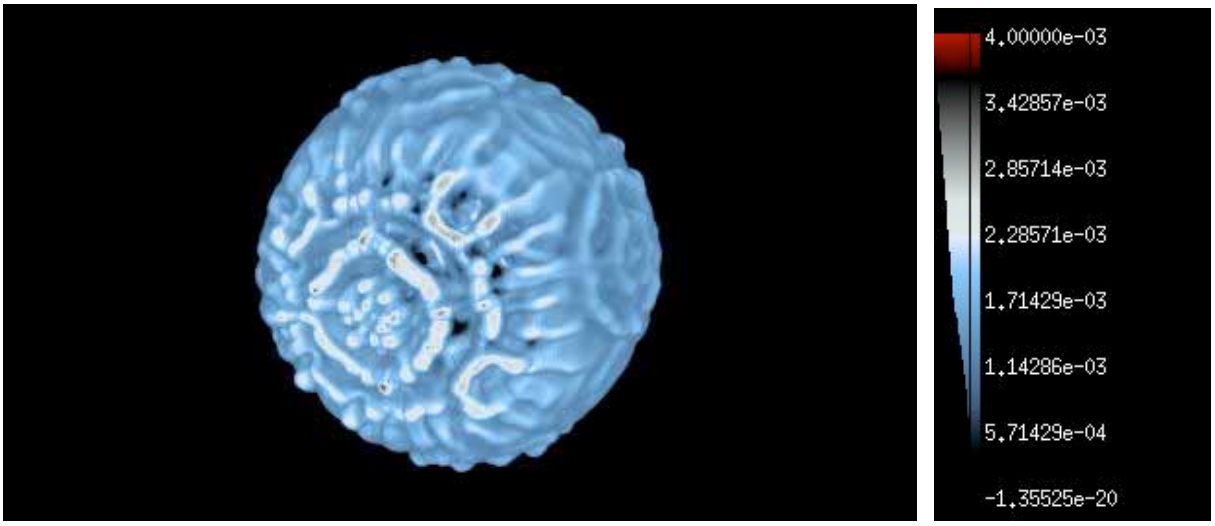

Figure 7. Volume rendering of the combustion Products surface at the beginning of the combustion process ($t = 70\,\mu s$) as simulated by the 3D AMR code (equilibrium model). Color palette of the concentration is shown at the right.

Figure 10 depicts the computed pressure history on the top wall, and compares it with four experimental pressure records obtained for an Al-SDF explosion in a cylindrical bomb calorimeter. Comparisons are encouraging. We believe that the $50\,\mu s$ delay of the second and third computed shocks is caused by afterburning of the PETN detonation products gases, which was neglected in these simulations. We plan to explore this and other two phase issues in future calculations.

The computed fuel history is depicted on Fig. 11. It shows that more than 96% of the Al is consumed during the 3 milliseconds of the simulation.

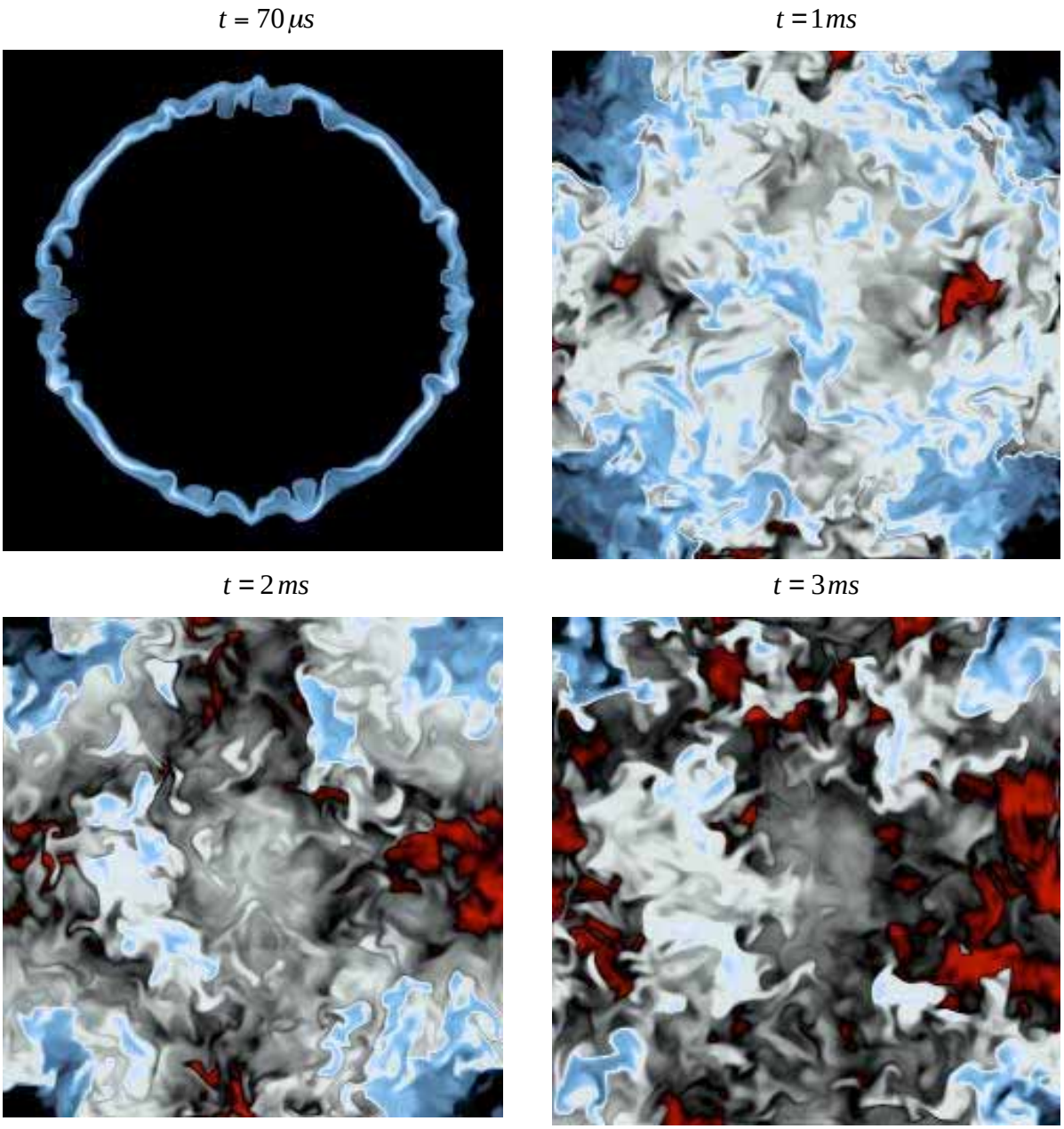

Figure 8. Cross-sectional views of the combustion Products concentration field in the mid-plane of the 6.4-liter cube at various times during the 3D AMR simulation (equilibrium model). Color palette is shown in Fig. 7.

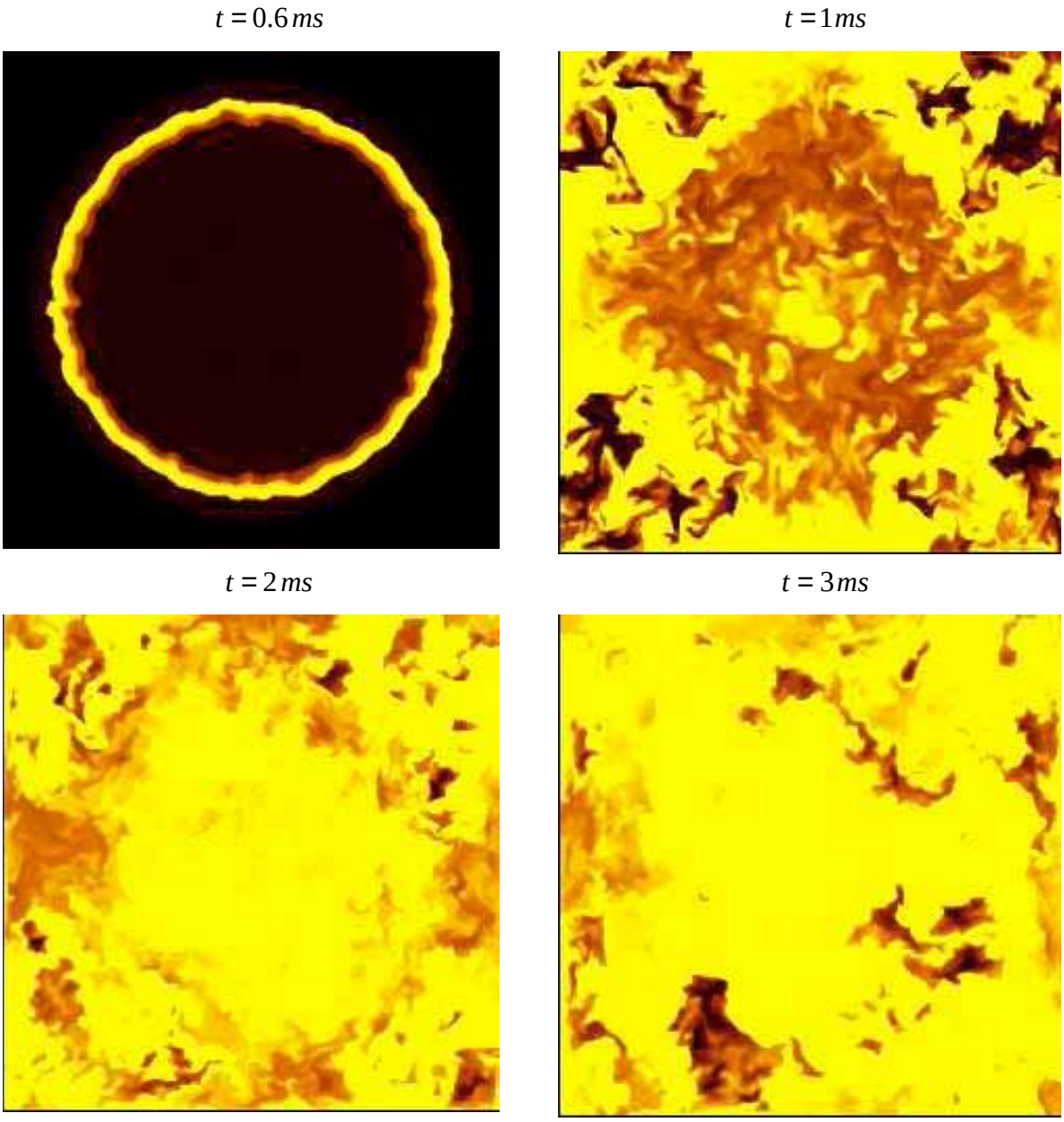

Figure 9. Cross-sectional views of the temperature field in the mid-plane of the 6.4-liter cube at various times during the 3D AMR simulation (equilibrium model).

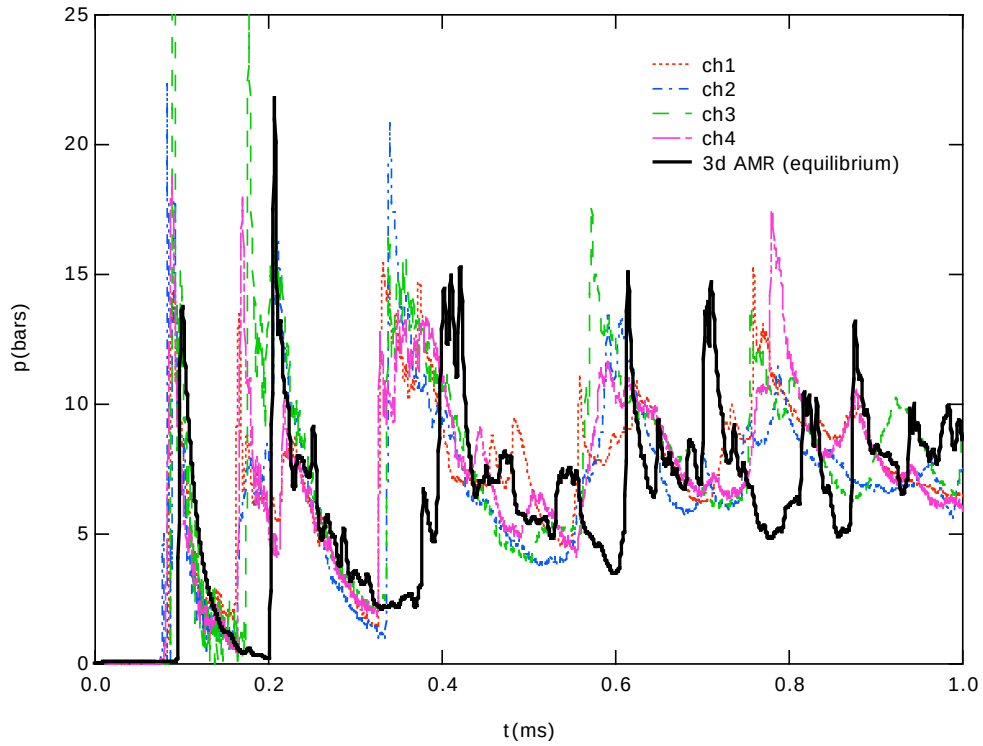

Figure 10. Comparison of pressure histories from the 3D-AMR simulation of Al-air combustion in a 6.4-liter cube with experimental pressure records from the 6.6-liter cylindrical calorimeter.

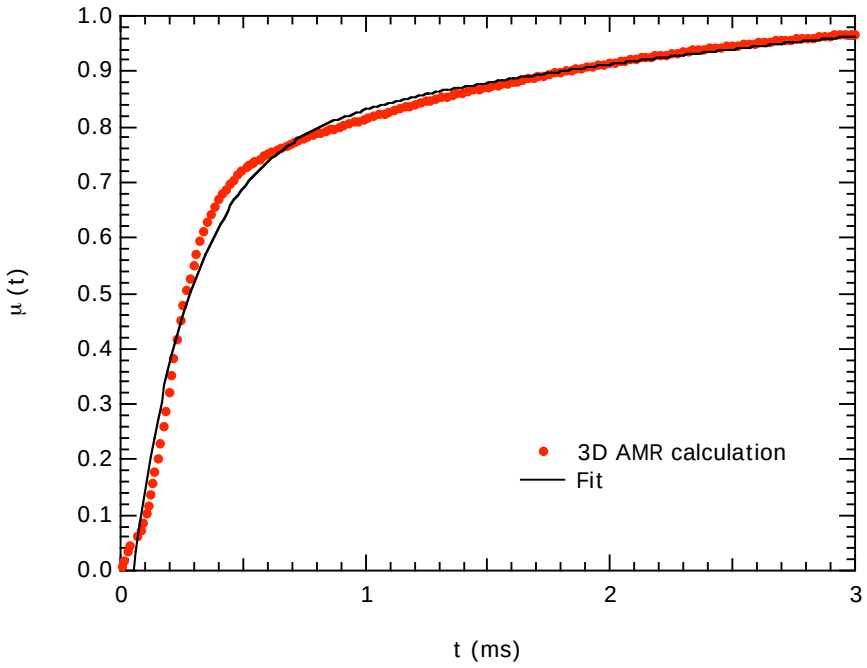

Figure 11. Mass fraction of fuel (Al) consumed from the 3D-AMR simulation. Results are fit by the function: $\mu(t) = 1.12 - 0.363e^{-0.284t} - 0.939e^{-4.20t}$.

SUMMARY AND CONCLUSIONS

Numerical simulations of the combustion of Aluminum particles in shock-dispersed-fuel explosions have been presented. For the problem studied, non-equilibrium effects, such as velocity and temperature slip between phases, seem to be most important during the initial expansion of the blast wave (i.e., during the *particle dispersion phase* of the problem). In the present case, the gas and particles rapidly equilibrated due to large inter-phase drag forces. During the *combustion phase* of the problem ($0.1ms < t < 3ms$), the two phases were in quasi-equilibrium. Consequently, combustion was modeled with the equilibrium-form of the 3D conservation laws (1)-(16). Visualization of the 3D fields confirmed that the computed solution was turbulent. Predicted pressure histories on the wall showed qualitative agreement with measurements. This suggests that the model produces burning rates that are similar to those in the experiments.

This is a non-premixed combustion problem (initially, fuel and oxidizer are physically separated), so the combustion rate is controlled by the mixing rate. During the particle dispersion phase, fuel and oxidizer are brought together by *ballistic mixing* (due to slip effects); then during the combustion phase, fuel and oxidizer are brought together by *turbulent mixing*. By using AMR, we are able to capture enough of the mixing scales to achieve physically realistic burning rates.

The proposed thermodynamic formulation models combustion as material transformations in the *Le Chatelier* plane. It provides a sharp (precise) description of thermodynamic states encountered during combustion of dilute Al-air mixtures at atmospheric pressures (1-10 bars). Being analytic, it is inherently fast and leads to efficient Equation of State routines especially suitable for 3d numerical simulations.

ACKNOWLEDGMENTS

This work was performed under the auspices of the U. S. Department of Energy by the University of California, Lawrence Livermore National Laboratory under Contract No. W-7405-Eng-48. It was sponsored by the Defense Threat Reduction Agency under IACRO # 06-40731. The LLNL document number is UCRL-ABS-224539

REFERENCES

1. P. Neuwald, H. Reichenbach and A. L. Kuhl, 2003, "Shock-Dispersed Fuel Charges—Combustion in Chambers and Tunnels", *Energetic Materials*, 34th ICT Conf, 13.1-13.14.
2. A. L. Kuhl, R. E. Ferguson and A. K. Oppenheim, 1999, "Gas-dynamics of Combustion of TNT Products in Air", *Archivum Combustionis* 19:1-4, 67-89.
3. R. I. Nigmatulin, 1987, **Dynamics of Multi-phase Flows**. Vol. 1. Moscow: Nauka, 464 pp.
4. B. Khasainov, A. L. Kuhl, S. Victorov and P. Neuwald, 2005, "Model of Non-Premixed Combustion of Al-Air Mixtures" *14th APS Meeting on Shock Compression of Condensed Matter*, Am. Ph. Soc. (in press).
5. W. Ingignoli 1999 *Etude de la formation et de la propagation des détonations dans des suspensions de particules d'aluminium en atmosphère oxydante ou réactive*. Thèse d'Université de Poitiers, France.
6. A. L. Kuhl, M. Howard and L. Fried, 1999, "Thermodynamic Model of Afterburning in Explosions" *Energetic Materials*, 34th ICT Conference, 74.1-74.14.
7. A. L. Kuhl, 2006, "Thermodynamic Model of Aluminum Combustion in SDF Explosions", *Energetic Materials*, 37th ICT Conference, Karsruhe, Germany.
8. J. B. Jones and G. A. Hawkins 1960 **Engineering Thermodynamics**: *An Introductory Textbook*, Wiley, New York, p. 405.
9. H. L. Brode, 1959, "Blast Wave from a spherical Charge", *Physics of Fluids*, 2(2), pp. 217-229.
10. J. Bell, M. Berger, J. Saltzman, and M. Welcome, 1994, "Three-dimensional Adaptive Mesh Refinement for Hyperbolic Conservation Laws"**,** *J. Comp. Phys*., **15** (1), pp. 127-138.
11. R.B. Pember, J.B. Bell, P. Colella, W.Y. Crutchfield & M. L. Welcome. 1995, "An Adaptive Cartesian Grid Method for Unsteady Compressible Flow in Irregular Regions". *J. Comp. Phys*., **120(2)**, pp. 278–304.
12. J. Boris, F. Grinstein, E. Oran, and R. Kolbe. 1992, "New insights into large eddy simulation". *Fluid Dynamics Research*, **10**, pp. 199-228.

APPENDIX: EQUATION OF STATE CONSTANTS

Table 1. Air EOS (10 bar): Piece-wise Quadratic Model\

Region *i*	a_A^i	b_A^i	c_A^i
1 (300—2,340K)	2.02768 E-5	0.16498	-71.9172
2 (2,340—3,700K)	1.34322 E-4	-0.41045	658.24424
3 (3,700—4,150K)	7.01281 E-5	0.11507	-403.36139
4 (4,150—4,530K)	-1.02084 E-4	1.53731	-3,340.674
5 (4,530—6,000K)	4.04923 E-5	0.11381	198.38643

Table 2. PETN detonation products EOS (CJ isentrope): Piece-wise Quadratic Model

Region *i*	a_{DP}^i	b_{DP}^i	c_{DP}^i
1 (300—2,340K)	3.31674 E-5	0.20867	-1,890.164
2 (2,340—3,700K)	5.97088 E-5	0.0377	-1,634.868
3 (3,700—4,150K)	1.9052 E-4	-0.89226	20.04935
4 (4,150—4,530K)	2.28177 E-4	-1.20053	651.0422
5 (4,530—6,000K)	1.78281 E-4	-0.774255	-248.616

Table 3. PETN-air combustion products EOS (10 bars): Piece-wise Quadratic Model

Region *i*	a_{CP}^i	b_{CP}^i	c_{CP}^i
1 (300—2,340K)	4.745 E-5	0.1549	-1,555.6
2 (2,340—3,700K)	4.6038 E-4	-1.7722	711.74
3 (3,700—4,150K)	4.9083 E-4	-1.841	558.87
4 (4,150—4,530K)	-6.1549 E-4	7.3463	-18,515.0
5 (4,530—6,000K)	-2.8216 E-4	3.8022	-9,254.5

Table 4. Al inert EOS: Piece-wise Quadratic Model

Region *i*	a_{Al}^i	b_{Al}^i	c_{Al}^i
1-5 (300—6,000K)	0	0.28128	-8.3895

Table 5. Al-Air combustion products EOS (10 bar): Piece-wise Quadratic Model

Region *i*	a_P^i	b_P^i	c_P^i
1 (300—2,340K)	1.76153E-5	0.20186	-1,553.62
2 (2,340—3,700K)	1.49115 E-5	0.2502	-1,554.5182
3 (3,700—4,150K)	0.00113	-7.95255	13,553.8
4 (4,150—4,530K)	0.00826	-67.29752	137,084.51
5 (4,530—6,000K)	5.03544 E-5	-0.07059	1,216.0279

Table 6. Molecular mass for components

Component	**condition**	**MW** (g/mole)
Air	p=10 bars, $T < 3{,}000K$	28.85
PETN detonation products	isentrope, $T = 1{,}800K$	28.76
PETN-air combustion products ($\sigma_s = 0.482$)	p=10 bars, $T_a = 3{,}200K$	27.75
Al-air combustion products ($\sigma_s = 4.03$)	p=10bars, $T_a = 4{,}120K$	40.78